Multi-objective Optimization of the 7075 Aluminum Alloy Milling Process: A Comparative Study of MOPSO, NSGA-II, SPEA2, and MOACO

Son Hoang [1], Cong Chi Tran [2], Van Tinh Pham [2], and Van Tuong Tran [2,*]

[1] Faculty of Electronics Engineering 1, Posts and Telecommunications Institute of Technology, Hanoi, Vietnam
[2] Faculty of Electromechanical and Civil Engineering, Vietnam National University of Forestry, Hanoi, Vietnam
Email: hoangson@ptit.edu.vn (S.H.); trancongchi_bk@yahoo.com (C.C.T.); tinhpv.vnuf@gmail.com (V.T.P.); tuongtv.vnuf@gmail.com (V.T.T.)
*Corresponding author

***Abstract*—This study investigated the influence of machining parameters and performed a comparative multi-objective optimization of surface roughness (*Ra*) and Material Removal Rate (MRR) in the milling of 7075 aluminum alloy using Multi-Objective Particle Swarm Optimization (MOPSO), Non-dominated Sorting Genetic Algorithm II (NSGA-II), Strength Pareto Evolutionary Algorithm 2 (SPEA2), and Multi-Objective Ant Colony Optimization (MOACO). Three machining parameters, including spindle speed (*S*), feed rate (*f*), and depth of cut (*d*), were considered. Analysis of Variance (ANOVA) results showed that *S* and *f* significantly affect *Ra* ($p < 0.05$), contributing 20.06% and 79.68%, respectively, while *f* and *d* are the most significant factors influencing MRR ($p < 0.05$), accounting for 45.01% and 40.11% of the total contribution. A predictive model for *Ra* developed using the Group Method of Data Handling (GMDH) demonstrated high predictive performance, with R^2 values of 0.9990 and 0.9962 for the training and validation datasets, respectively. Comparative analysis indicated that NSGA-II produced the most stable solutions, whereas SPEA2 and MOACO exhibited less balanced performance, and MOPSO achieved rapid convergence with relatively dispersed solutions. Experimental validation of *Ra* and analytical verification of MRR confirmed the reliability of the proposed framework, with mean deviations of 6.5% and 0.37%, respectively. Unlike prior investigations that examined individual algorithms or lacked integrated experimental assessment, this study presents a systematic cross-algorithm evaluation under identical machining conditions. The proposed framework integrates statistical contribution analysis, predictive modeling, and experimental validation, thereby establishing a robust and practically applicable approach for multi-objective milling optimization.**

***Keywords*—multi-objective optimization, milling, Multi-Objective Particle Swarm Optimization (MOPSO), Non-dominated Sorting Genetic Algorithm II (NSGA-II), Strength Pareto Evolutionary Algorithm 2 (SPEA2), Multi-Objective Ant Colony Optimization (MOACO)**

I. Introduction

In advanced manufacturing environments, optimization of machining processes is widely regarded as a prerequisite for sustaining industrial competitiveness and ensuring long-term operational sustainability [1, 2]. The aerospace, automotive, and defense sectors increasingly demand components with exceptional mechanical properties, dimensional accuracy, and surface integrity while requiring cost-effective and environmentally sustainable production methods. Among high-performance materials, 7075 aluminum alloy stands as a paradigmatic example of an engineering material that offers high specific structural performance, strong fatigue durability, and good processability, making it indispensable in weight-critical applications such as aircraft structures, military equipment, and high-performance automotive components [3–5]. However, the machining process of this alloy is a multifaceted interaction of conflicting goals, such as surface quality, tool life, material removal rate, energy efficiency, manufacturing costs, etc, that require close consideration to realize optimum performance.

Traditional single-objective optimization approaches have proven inadequate in addressing the inherent multi-criteria nature of complex manufacturing processes, as they inevitably prioritize one performance metric at the expense of others [6, 7]. This limitation has catalyzed significant research interest in Multi-Objective Optimization (MOO) techniques that simultaneously consider multiple competing objectives and provide a spectrum of optimal solutions representing different trade-offs, commonly known as the Pareto front [8].

Recent advances in computational intelligence and evolutionary algorithms have fundamentally transformed

Manuscript received January 6, 2026; revised January 23, 2026; accepted February 26, 2026; published April 23, 2026.

the domain of manufacturing process optimization by enabling more efficient exploration of vast parameter spaces and handling of non-linear, multi-modal, and discontinuous objective functions that characterize real-world machining processes [9–11]. Among these techniques, Multi-Objective Particle Swarm Optimization (MOPSO), Non-dominated Sorting Genetic Algorithm II (NSGA-II), Strength Pareto Evolutionary Algorithm 2 (SPEA2), and Multi-Objective Ant Colony Optimization (MOACO) have emerged as particularly promising approaches due to their demonstrated effectiveness in solving complex engineering optimization problems. Each algorithm utilizes distinct mechanisms for population evolution, fitness evaluation, diversity preservation, and convergence to the Pareto-optimal front, potentially leading to different optimization outcomes for the same manufacturing scenario. Specifically, MOPSO extends the multi-objective domain by incorporating mechanisms for non-dominated solution archiving and leader selection, exploiting the efficiency of swarm intelligence in navigating complex search spaces [12–14]. NSGA-II utilizes a rapid non-dominated sorting mechanism, with an elitism-based strategy and crowding distance calculation to identify and maintain a well-spread approximation of the Pareto front [15–17]. SPEA2 emphasizes fine-grained fitness assignment based on dominance strength and nearest neighbor density estimation, potentially offering advantages in maintaining solution diversity throughout the evolutionary process [18, 19]. MOACO adapts the ant colony metaphor to multi-objective problems by employing multiple pheromone matrices and heuristic information sources corresponding to different objectives, potentially excelling in problems with a discrete or combinatorial structure [20].

Numerous researchers have applied MOO to the optimization of machining processes and obtained certain results. Guo *et al.* [21] applied the RSM combined with the MOPSO algorithm to optimize milling parameters under micro-scale lubrication conditions. Their findings revealed a relative error of 8.14% between the predicted and experimentally measured tangential cutting forces. Luis-Pérez [22] developed a multi-objective optimization approach driven by PSO to refine operating parameters during the sinker EDM of Inconel® alloy. This method enabled the effective creation of machining technology tables tailored for EDM applications, demonstrating its practical efficiency and utility. NSGA-II is a widely adopted evolutionary algorithm for addressing optimization problems involving multiple, often conflicting objectives. Tran [23] optimized *Ra* and Material Removal Rate (MRR) for SKD11 material during milling using the Taguchi Orthogonal Array (TOA) and the GMDH for predictive modeling. The NSGA-II technique generated 70 Pareto solutions. The model achieved an R^2 of 0.981, with validation deviations under 10.3%, offering a practical approach to enhance productivity and quality. Lu *et al.* [24] also applied this algorithm to determine optimal cutting conditions in the micro-milling of nickel-based alloy 718, aiming to obtain lower *Ra* and higher MRR. Several other studies using this algorithm for machining optimization have also been published [25–29]. Additionally, SPEA2 and MOACO have been applied for optimization in other studies [30–33].

In the authors' previous work, a comparative performance analysis of three single-objective metaheuristic optimization algorithms was conducted for minimizing surface roughness in aluminum alloy milling. A highly accurate predictive model for *Ra* was developed using GMDH and integrated into the optimization framework. The results indicated that PSO exhibited superior convergence speed, stability, and robustness compared with GA and SA, demonstrating the effectiveness of population-based metaheuristic algorithms for machining parameter optimization. However, that study was limited to a single-objective formulation and did not resolve the conflicting relationship between surface quality and productivity encountered in practical machining processes.

Although MOO techniques have achieved significant results in research and production, their application in the specific context of 7075 aluminum alloy milling is still limited. Most existing studies focus on applying a single algorithm or a limited comparison of two techniques, typically under differing process conditions and materials. This approach limits the generalizability of results and the practicality of optimization techniques. Therefore, comparative studies still need to provide a complete performance analysis of different MOO algorithms when applied to solve the same problem to establish clear guidelines for algorithm selection.

This study addresses the research gap described above by developing an experimental framework to evaluate the performance of MOPSO, NSGA-II, SPEA2, and MOACO in the context of milling 7075 aluminum alloy. The optimization focuses on three critical machining parameters, including spindle speed (*S*), feed rate (*f*), and depth of cut (*d*), and their influence on two conflicting machining objectives, *Ra* and MRR. The GMDH approach was employed to construct a predictive model for estimating the *Ra* objective function. Through a detailed comparative analysis of the four algorithms in terms of convergence behavior, solution quality, and trade-off characteristics, this study provides practical insights into their applicability. This work extends our previous study on single-objective surface roughness optimization by incorporating material removal rate and formulating a multi-objective optimization framework using advanced algorithms. Accordingly, the proposed approach aims to provide a more comprehensive and practical optimization strategy for milling processes. The findings of this work are expected to provide additional insights into the comparative evaluation of these four MOO algorithms in practical manufacturing contexts.

II. Materials and Methods

A. Workpiece, Machine and Cutting Tool

The workpieces used in the experiments were rectangular blocks with dimensions of (100 × 65 × 10 ±1)

mm. According to the manufacturer's specifications, the 7075-aluminum alloy material had a density of approximately 2.81 g/cm³. The material is predominantly composed of aluminum (87.1%–91.4%), with chromium and copper present in the ranges of 0.18%–0.28% and 1.2%–2.0%, respectively.

The samples were machined using a MORI SEIKI MV JUNIOR machining center with a Fanuc 10M control system, utilizing Venus GPX coolant at approximately 2.5%–3.0% concentration to enhance cutting conditions (Fig. 1). The experiments were conducted using a solid carbide end mill (10 mm diameter) incorporating three flutes and a 55° cutting angle.

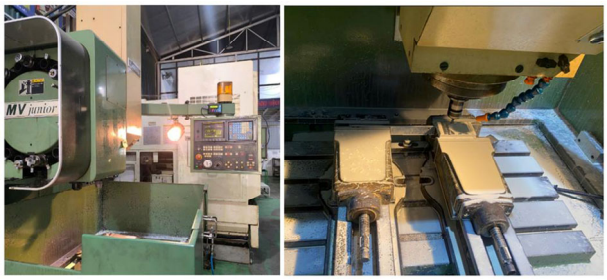

Fig. 1. MORI SEIKI MV JUNIOR machine used in the experiment.

TABLE I. MACHINING CONDITION ACCORDING TO ORTHOGONAL ARRAY L25 (5^3)

No	*S* (rpm)	*f* (mm/rev)	*d* (mm)
1	3000	0.2	0.25
2	3000	0.4	0.50
3	3000	0.6	0.75
4	3000	0.8	1.00
5	3000	1.0	1.25
6	3500	0.2	0.50
7	3500	0.4	0.75
8	3500	0.6	1.00
9	3500	0.8	1.25
10	3500	1.0	0.25
11	4000	0.2	0.75
12	4000	0.4	1.00
13	4000	0.6	1.25
14	4000	0.8	0.25
15	4000	1.0	0.50
16	4500	0.2	1.00
17	4500	0.4	1.25
18	4500	0.6	0.25
19	4500	0.8	0.50
20	4500	1.0	0.75
21	5000	0.2	1.25
22	5000	0.4	0.25
23	5000	0.6	0.50
24	5000	0.8	0.75
25	5000	1.0	1.00

B. Experimental Design

The TOA method was employed to establish the appropriate number of experimental runs. Three machining parameters were selected for investigation, including *S*, *f*, and *d*. Each of these parameters was divided into five levels to capture a comprehensive range of process conditions. Specifically, spindle speed varied from 3000 to 5000 rpm, feed per revolution ranged from 0.2 to 1.0 mm/rev, and depth of cut varied between 0.25 and 1.25 mm. With three input machining parameters, each with five levels, a total of 25 experimental runs were determined using an L25 orthogonal array structure. These experiments are detailed in Table I.

All milling experiments were conducted under a full-slot end-milling strategy, where the radial depth of cut was equal to the tool diameter. The axial depth of cut varied according to the experimental design. Down-milling was adopted for all machining tests to ensure stable cutting conditions and consistent surface generation.

C. Measurement and Calculation Methods for Performance Parameters

Ra was measured with a Mitutoyo TR200 portable profilometer fitted with a diamond-tipped stylus of a 5 μm radius. A cutoff length of 0.8 mm was applied, and the total evaluation length was set to 4.0 mm, corresponding to five consecutive cutoff intervals. All measurements were performed perpendicular to the feed direction to capture the dominant surface texture generated by the milling process. For each experimental condition, three *Ra* measurements were collected at different positions, and the mean value was used for analysis.

MRR was not measured experimentally but was deterministically calculated from the cutting parameters using Eq. (1). Therefore, MRR represents a theoretical productivity indicator derived from machining kinematics rather than a directly measured response.

$$MRR = S \times f \times d \times a \ (mm^3/min) \quad (1)$$

where *S* denotes the spindle speed (rpm), *f* is the feed per revolution (mm/rev), *d* represents the axial depth of cut (mm), and *a* is the radial width of cut (mm). In this study, the radial width of cut was fixed and equal to the tool diameter (10 mm), corresponding to a full-slot milling condition.

D. Methodology

1) Workflow for machining process optimization

The optimization of machining process parameters was carried out through a structured workflow integrating experimental investigation, predictive modeling, and multi-objective optimization. First, a predictive model for *Ra* was developed using the GMDH approach and employed as the first objective function. Second, MRR was calculated from an analytical formulation and served as the other objective. Subsequently, multi-objective optimization algorithms were applied to identify Pareto-optimal combinations of cutting parameters. Finally, representative solutions from the Pareto front were selected and validated through additional machining experiments to assess the effectiveness of the optimized process parameters. This approach enabled the systematic optimization of machining parameters while maintaining practical relevance for manufacturing applications.

2) Group Method of Data Handling (GMDH)

The GMDH is a family of inductive self-organizing algorithms used for modeling complex systems, prediction, and pattern recognition. This method operates

on the principle of a multi-layered network architecture, where each layer comprises a set of interconnected "neurons" through polynomial functions. This structure facilitates the mapping of input-output relationships. The primary task of GMDH is to approximate an unknown or complex polynomial function. Specifically, the goal is to find a surrogate function ($\hat{f}$) that can accurately estimate the output ($\hat{y}$ = f(Z)) for a given input vector $Z = (z_1, z_2, ..., z_n)$, such that the estimated output closely approximates the actual output (y) of the system under study.

Selecting a suitable GMDH neural structure that minimizes the deviation between estimated and actual responses poses a significant challenge. Utilizing a discrete expansion of the Volterra functional series, the mapping between the input parameters and the corresponding outputs was formulated as indicated in Eq. (2).

$$y = b_0 + \sum_{i=1}^{n} b_i z_i + \sum_{i=1}^{n}\sum_{j=1}^{n} b_{ij} z_i z_j + \sum_{i=1}^{n}\sum_{j=1}^{n} n \sum_{k=1} b_{ijk} z_i z_j z_k + \ldots \quad (2)$$

where b_0, b_i, b_{ij}, b_{ijk}, ... are coefficients characterizing the level of interaction and influence of input factors on the system output. Fig. 2 depicts the structure of a GMDH model utilizing three input variables: z_i, z_j, and z_k.

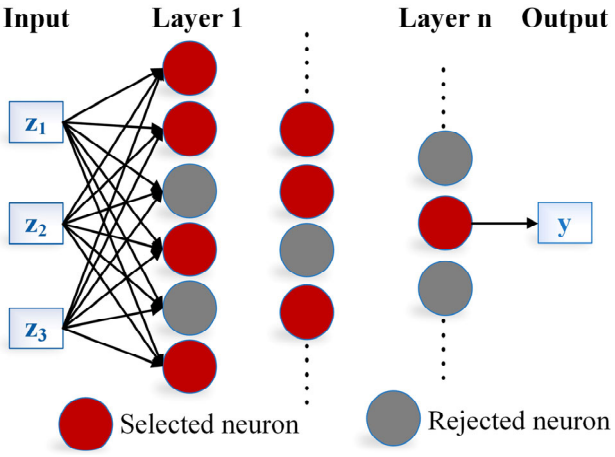

Fig. 2. Structure of the GMDH model with three machining input parameters.

GMDH networks are constructed upon a quadratic polynomial representation initially developed by Ivakhnenko [34]. However, various polynomial types, including quadratic, tri-quadratic, bilinear, and third-order polynomials, etc, are also employed in designing predictive models. The determination of a suitable polynomial model is governed by many factors, such as the input parameters, polynomial complexity, and minimization of the objective function error.

In this study, GMDH was employed to establish the nonlinear relationship between machining parameters and surface roughness. The input variables of the model consisted of *S*, *f*, and *d*, while the output variable was the *Ra*. The GMDH approach was selected because it is well suited for modeling nonlinear relationships in machining processes with limited experimental data. Unlike black-box models, GMDH provides an explicit analytical formulation, which improves model interpretability and facilitates its integration into the subsequent multi-objective optimization framework.

Due to the limited sample size in this study, it is challenging to obtain a highly accurate model if the training and validation data are divided mechanically. Therefore, a 10-fold cross-validation method was used to objectively evaluate the predictive model and minimize bias associated with using a single training and validation dataset. Specifically, the data was divided into 10 equal sets, with nine sets used to train the model in each iteration and the remaining set used for validation. This method ensures that each set data will be used for training and validation at least once and provides a more accurate and larger evaluation of the model.

During the GMDH model construction, different polynomial neuron structures were examined to identify the most suitable predictive formulation. Specifically, eight candidate functions, including Linear (2 variables), Linear (3 variables), Quadratic (1 variable), Quadratic (2 variables), Cubic (1 variable), Double (2 variables), and Triple (3 variables), were evaluated and compared. To control model complexity and avoid overfitting, the network depth was restricted to a maximum of 30 layers, while the polynomial degree was capped at 16. These settings enabled the model to represent complex nonlinear relationships without compromising computational efficiency. The training process was terminated based on an error convergence criterion with a tolerance of 10^{-4}, such that further reductions in prediction error became negligible.

The predictive performance of each GMDH model was evaluated using the coefficient of determination (R^2), Root Mean Square Error (RMSE), and Mean Absolute Percentage Error (MAPE), as defined in Eqs. (3)–(5). The model exhibiting the best overall performance based on these statistical indices was selected for the optimization analysis step.

$$R^2 = 1 - \left[\frac{\sum_{i=0}^{n}(y_{predict} - y_{Actual})^2}{\sum_{i=0}^{n}(y_{Actual})^2}\right] \quad (3)$$

$$MAPE = 1 - \left[\frac{\sum_{i=0}^{n}|y_{predict} - y_{Actual}|}{n \times \sum_{i=0}^{n}(y_{Actual})}\right] \quad (4)$$

$$RMSE = \sqrt{\frac{\sum_{i=0}^{n}(y_{predict} - y_{Actual})^2}{n}} \quad (5)$$

3) Multi-objective optimization using MOPSO

MOPSO extends the conventional PSO framework to address multi-objective optimization problems, drawing inspiration from collective behaviors observed in biological systems such as bird flocks and fish schools [13]. The procedure starts with the generation of an initial swarm, in which each particle represents a candidate solution within the search domain. The particle's

state is characterized by its position and velocity vectors, denoted as X_i and V_i, respectively, as defined in Eqs. (6) and (7).

$$V_i^{(t+1)} = \omega \times V_i^{(t)} + C_1 \times r_1 \times (P_i^{best} - X_i^{(t)}) + C_2 \times r_2 \times (G_i^{best} - X_i^{(t)}) \quad (6)$$

$$X_i^{(t+1)} = X_i^{(t)} + V_i^{(t+1)} \quad (7)$$

where ω represents the inertia weight, C_1 and C_2 denote the individual and social coefficients, respectively, and r_1 and r_2 are random numbers uniformly distributed between 0 and 1.

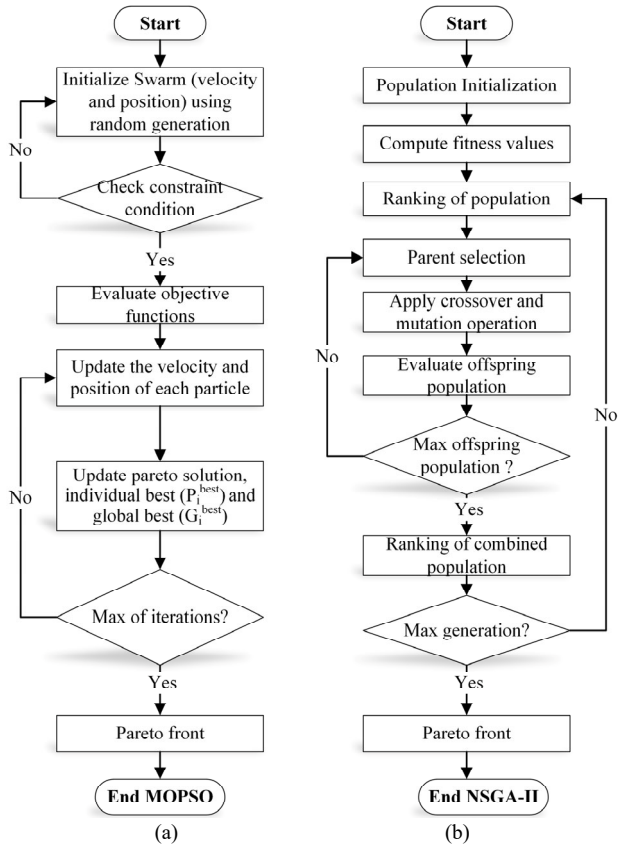

Fig. 3. Flowcharts of the (a) MOPSO; and (b) NSGA-II algorithms.

MOPSO performs a multi-objective search to approximate the Pareto front, where each solution reflects a compromise among different objectives. Accordingly, each particle retains its personal best position, while an external archive is maintained to store non-dominated solutions. Although the position and velocity updating mechanisms follow the conventional PSO scheme, a leader (L) selection strategy is incorporated to choose a guiding solution from the Pareto repository. The velocity update formulation adopted in MOPSO is provided in Eq. (8), and the overall procedural framework is depicted in Fig. 3(a).

$$V_i^{(t+1)} = \omega \times V_i^{(t)} + C_1 \times r_1 \times \left(P_i^{best} - X_i^{(t)}\right) + C_2 \times r_2 \times \left(L - X_i^{(t)}\right) \quad (8)$$

4) Multi-objective optimization using NSGA-II

NSGA-II is a multi-objective optimization method based on genetic principles. This algorithm is designed to solve optimization problems with multiple objectives [35]. The process of NSGA-II begins with the initialization of a population of candidate solutions. The individuals are evaluated and classified into Pareto fronts through non-dominated sorting, which ranks non-dominated solutions into different fronts. Superior individuals are then selected as parents for the next generation. Then, the genetic operations, including crossover and mutation, are used to generate offspring individuals. This operation enhances the exploration of the search space and maintains population diversity. All offspring individuals are evaluated and validated to ensure their number does not exceed a defined maximum value. The merged population of parents and offspring is then reclassified and evaluated once more. This evolutionary cycle proceeds until a predefined termination condition is met, commonly specified by a maximum number of generations or convergence of the population. Upon completion, the algorithm yields a Pareto-optimal solution set comprising non-dominated individuals that capture the trade-offs among the objectives. The steps of NSGA-II are illustrated in Fig. 3(b).

5) Multi-objective optimization using SPEA2

SPEA2 integrates evolutionary operators with Pareto-based selection mechanisms [18]. The procedure begins with the initialization of a population consisting of feasible candidate solutions. After initialization, variation operators such as mutation and crossover are employed to generate new individuals, promoting broader exploration of the search space. Then, the algorithm evaluates the strength and fitness of each individual to identify how well it performs in optimizing the objectives.

Based on these fitness values, individuals are selected to contribute to the next generation, and a Pareto archive, which stores non-dominated solutions, is updated to keep track of the best solutions found. This process is repeated until a stopping criterion is met, as illustrated in the SPEA2 procedure shown in Fig. 4(a).

6) Multi-objective optimization using MOACO

MOACO is a metaheuristic approach derived from the foraging behavior of ant colonies and it has been modified to address MOO problems [20]. Unlike single-objective ACO, which aims to find a single best path, MOACO approximates the Pareto front by generating a diverse set of non-dominated solutions.

The MOACO procedure begins with the generation of an ant population. Each ant generates potential solutions, evaluates them based on objective functions, and contributes to updating the Pareto archive. In every iteration, the ants update the pheromone levels on the paths traveled, affecting the subsequent ants to find improved solutions. The procedure is repeated until the maximum iterations (Iteration-max) is reached. Once this condition is met, the algorithm terminates and outputs the optimal solutions from the Pareto archive, which represent the best

trade-offs among the objectives [36]. The steps of MOACO are illustrated in Fig. 4(b).

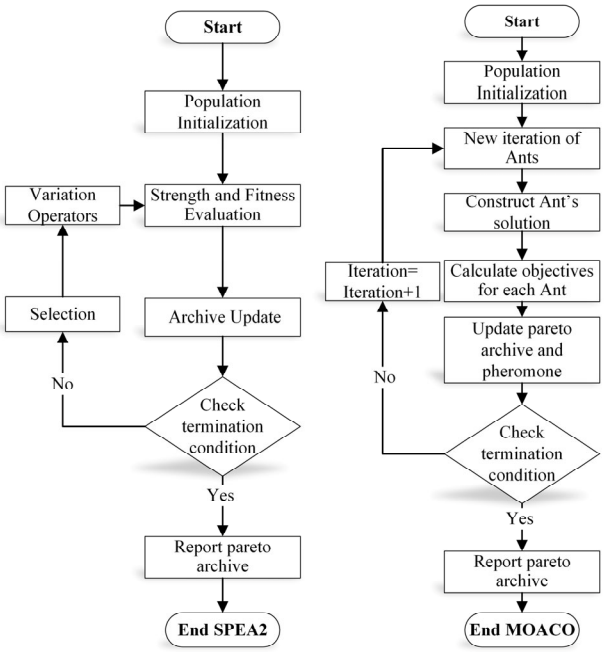

Fig. 4. Flowcharts of the (a) SPEA2; and (b) MOACO algorithms.

III. Results and Discussion

A. Effect of Machining Process Parameters on Ra and MRR

An ANOVA was conducted to assess the effects of *S*, *f* and *d* on *Ra* and MRR. As summarized in Table II, *f* was identified as the dominant factor, accounting for 79.68% of the total variance. From a machining mechanism perspective, increasing *f* leads to a larger undeformed chip thickness, which increases cutting forces and enhances the likelihood of vibration and chatter. In addition, higher feed rates amplify the helical tool marks on the machined surface, resulting in deeper and wider grooves and, consequently, higher *Ra*.

S was also statistically significant ($p < 0.001$), contributing 20.06% of the total variance. This is because higher cutting speeds can improve surface quality by reducing the built-up edge and decreasing cutting forces. However, although d is known to influence surface characteristics through its role in material removal and chip formation, its impact was limited in this study. The parameter *d* showed no statistically significant effect ($p = 0.075$). This result may be attributed to the narrowly selected range of *d*, which failed to generate sufficient variation to produce a statistically significant effect on *Ra*.

Since MRR was analytically calculated rather than experimentally measured, the ANOVA analysis was conducted to evaluate the sensitivity of cutting parameters to the theoretical material removal capability. The results showed that *f* was highly significant ($p < 0.001$) and the most influential factor affecting the calculated MRR, accounting for 45.01% of the total variation, which is consistent with the analytical formulation of MRR. This finding aligns with theoretical expectations, as increasing *f* directly increases the amount of material removed within a given time interval. The parameter *d* also exhibited statistical significance ($p < 0.001$) and was identified as the second most influential factor, contributing 40.11% of the total variation. This is because deeper cuts engage more material in a single pass, thereby increasing the removal rate. However, *S* had a negligible effect on MRR ($p = 0.373$), contributing only 4.17% to the total variation. Therefore, the ANOVA results for MRR should be interpreted as a sensitivity analysis of cutting parameters based on the analytical MRR formulation, rather than as an assessment of experimental variability. Fig. 5 illustrates the influence of the milling parameters on *Ra* (a, b, c) and the analytically calculated MRR (d, e, f).

The observed trade-off between *Ra* and MRR can be explained by fundamental machining mechanisms, whereby higher feed rates and depths of cut increase productivity at the expense of surface quality due to increased chip thickness and cutting forces. This inherent trade-off provides the physical basis for the multi-objective optimization and Pareto-based solution selection.

TABLE II. ANOVA Results for *Ra* and MRR

Responses	Source	DF	Seq SS	Contribution (%)	Adj SS	Adj MS	*F*	*p*
Ra	*S*	4	0.089	20.06	0.089	0.022	453.3	0
	f	4	0.353	79.68	0.353	0.088	1800.5	0
	d	4	0.001	0.12	0.001	0	2.8	0.075
	Error	12	0.001	0.13	0.001	0	-	-
	Total	24	0.443	100.00	-	-	-	-
MRR	*S*	4	1.60E+08	4.20	1.60E+08	3.90E+07	1.17	0.373
	f	4	1.70E+09	45.00	1.70E+09	4.20E+08	12.6	0
	d	4	1.50E+09	40.10	1.50E+09	3.80E+08	11.23	0.001
	Error	12	4.00E+08	10.70	4.00E+08	3.30E+07	-	-
	Total	24	3.70E+09	100.00	-	-	-	-

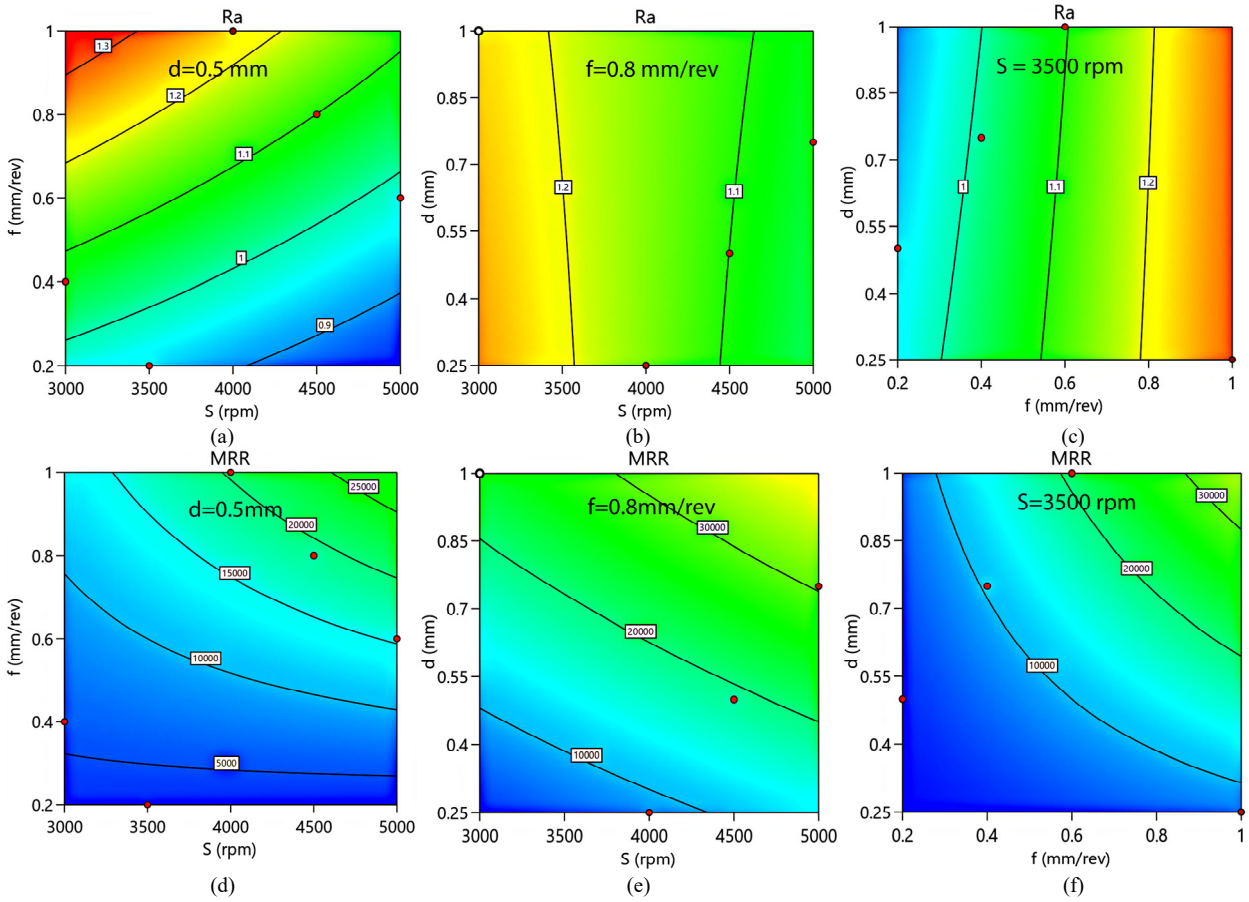

Fig. 5. Effects of milling parameters on *Ra* and MRR: (a) *S* and *f* for *Ra*; (b) *S* and *d* for *Ra*; (c) *f* and *d* for *Ra*; (d) *S* and *f* for MRR; (e) *S* and *d* for MRR; and (f) *f* and *d* for MRR.

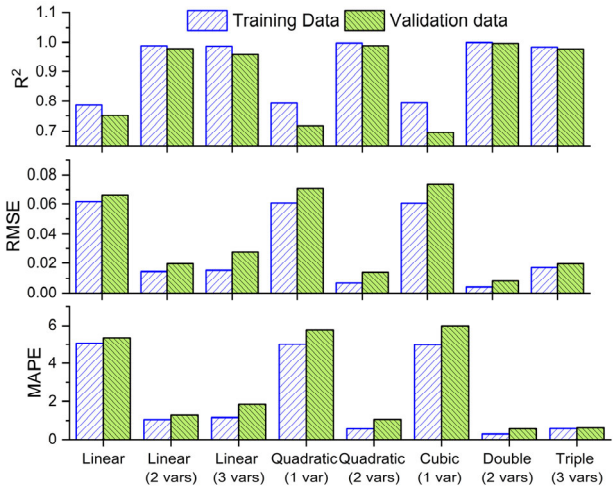

Fig. 6. Performance indicators of the GMDH model using different types of functions.

B. GMDH Model Performance Evaluation

The predictive performance of the candidate GMDH models was evaluated and compared, as illustrated in Fig. 6. The predictive performance of these models was assessed using R^2, RMSE, and MAPE. The results indicate that the Double (2 variables) function demonstrated the highest predictive performance. Specifically, it achieved an R^2 value of 0.9990 on the training set and 0.9962 on the validation set, indicating good capability in capturing the relationship between machining parameters and *Ra*. Furthermore, the RMSE and MAPE of this model were also the lowest among all eight functions used, reflecting minimal prediction error and high accuracy.

The analysis demonstrates that the Double (2 variables) function provides superior capability in representing the nonlinear relationships governing the studied milling operation. Thus, this predictive model is selected to serve as the objective function in multi-objective optimization together with MRR using MOPSO, NSGA-II, SPEA2, and MOACO. The GMDH model equations for *Ra* using the Double (2 variables) function are presented in Eq. (9):

$$\begin{aligned} R_{a2} &= 0.389687 + 0.425567 \times d + 0.011968 \\ &\times d^2 + 0.000362 \times S - 0.000124 \times d \times S \\ R_{a3} &= 1.103357 + 0.2606 \times f + 0.169483 \times f^2 \\ &-0.000044 \times S - 3.871179 \times 10^{-9} \\ &\times S^2 - 0.000012 \times f \times S \\ R_{a1} &= -0.580249 + 1.130448 \times R_{a2} - 0.386204 \\ &\times R_{a2}^2 + 0.97446 \times R_{a3} + 0.161984 \times R_{a3}^2 \\ &-0.302019 \times R_{a2} \times R_{a3} \\ Ra &= 0.640378 + 0.541213 \times f \\ &+0.069943 \times f^2 - 0.515667 \times R_{a1} + 0.883799 \\ &\times R_{a1}^2 - 0.593214 \times f \times R_{a1} \end{aligned} \quad (9)$$

Although the obtained R^2 values are high, the use of 10-fold cross-validation ensures that model performance is

evaluated on unseen data, thereby reducing the risk of overfitting. The small difference between the training and validation R^2 values further indicates that the model maintains consistent predictive performance.

Nevertheless, the limited dataset size may still introduce a degree of overfitting, which constitutes a limitation of the present study and should be addressed in future work through the use of larger experimental datasets.

C. Multi-objective Optimization

The optimization model was formulated to minimize *Ra* and maximize MRR. To maintain a consistent minimization framework across all optimization algorithms, the second objective was implemented by minimizing the negative value of MRR. All four algorithms (MOPSO, NSGA-II, SPEA2, and MOACO) were executed using the same objective formulations and identical search space boundaries to ensure a fair comparison. The decision variables were constrained within the ranges defined in Table III. No additional constraints were imposed during the optimization process.

TABLE III. INPUT PARAMETERS AND OBJECTIVES OF *RA* AND MRR

Input			Output	
Parameter	**Low level**	**High level**	**Parameter**	**Objective**
S (rpm)	3000	5000	MRR	Max MRR Eq. (1)
f (mm/rev)	0.20	1.00	*Ra*	Min *Ra* (Eq. 9)
d (mm)	0.25	1.25	-	-

For all four algorithms, the maximum number of generations (or iterations) was fixed at 600. The population size was set to 60, defining the number of individuals, particles, or ants per generation. For MOPSO, several specific parameters were defined, including an initial inertia weight of 0.9, a damping ratio of 0.995 and both personal and social acceleration coefficients set to 1.5. Additionally, MOPSO includes a grid expansion coefficient of 0.1 and a deletion pressure for archive members set to 2. In contrast, NSGA-II and SPEA2 utilize crossover and mutation probabilities, both set at 0.8 and 0.333, respectively. They also share a crossover distribution index of 20 and a polynomial mutation distribution index of 20. SPEA2 further specifies a neighbor count for density estimation set to 10. For MOACO, a mutation probability of 0.333 and a mutation distribution index of 20 were defined, along with a density neighbor count of 7. The archive size for storing non-dominated solutions was set to 60 for both MOPSO, SPEA2, and MOACO while NSGA-II does not utilize an archive in this context.

All algorithm-specific parameters were selected based on commonly adopted values reported in the literature and preliminary trials to ensure stable convergence behavior [37–40]. No algorithm-specific parameter fine-tuning was performed, as the objective of this study was to comparatively evaluate the general optimization behavior of the algorithms under consistent conditions rather than to maximize the performance of any single method. These parameter settings allow each algorithm to operate under comparable conditions and support a fair performance comparison. It should be noted that, due to the inherent structural and operational differences among the algorithms, such a comparison is necessarily relative rather than absolutely uniform, which is a common and accepted limitation in comparative optimization studies.

The Pareto results for the four MOO algorithms, MOPSO, NSGA-II, SPEA2, and MOACO, were presented in Fig. 7. Specifically, the MOPSO results indicated that the minimum values of *S*, *f*, and *d* were 5000 rpm, 0.20 mm/rev, and 0.25 mm, respectively, with *Ra* of 0.644 µm and MRR of 2500 mm³/min. The maximum values were achieved when *S* was 5000 rpm, *f* was 1.00 mm/rev, and *d* was 1.25 mm, resulting in *Ra* of 0.930 µm and MRR of 62500 mm³/min. For NSGA-II, the minimum values occurred with *S* at 4994.2 rpm, *f* at 0.25 mm/rev, and *d* at 1.08 mm, with *Ra* of 0.693 µm and MRR of 15590.79 mm³/min. The maximum values were 4996.4 rpm for *S*, 0.73 mm/rev for *f*, 1.25 mm for *d*, with *Ra* of 0.842 µm and MRR of 45326.94 mm³/min.

SPEA2 achieved a minimum with *S* at 4866.7 rpm, *f* at 0.24 mm/rev, and *d* at 1.10 mm, corresponding to *Ra* of 0.689 µm and MRR of 14162.40 mm³/min. The maximum values for SPEA2 were 4999.9 rpm for *S*, 0.88 mm/rev for *f*, 1.25 mm for *d*, with *Ra* of 0.891 µm and MRR of 54623.80 mm³/min. Lastly, for MOACO, the minimum values were found when *S* was 4923.5 rpm, *f* was 0.33 mm/rev, and *d* was 0.90 mm, with *Ra* of 0.705 µm and MRR of 14623.13 mm³/min. The maximum values for MOACO were *S* at 4986.5 rpm, *f* at 0.86 mm/rev, *d* at 1.24 mm, with *Ra* of 0.885 µm and MRR of 52850.70 mm³/min. These results demonstrated the range of optimal values that each algorithm could achieve in the MOO process, while emphasizing the ability of each algorithm to balance *Ra* and MRR.

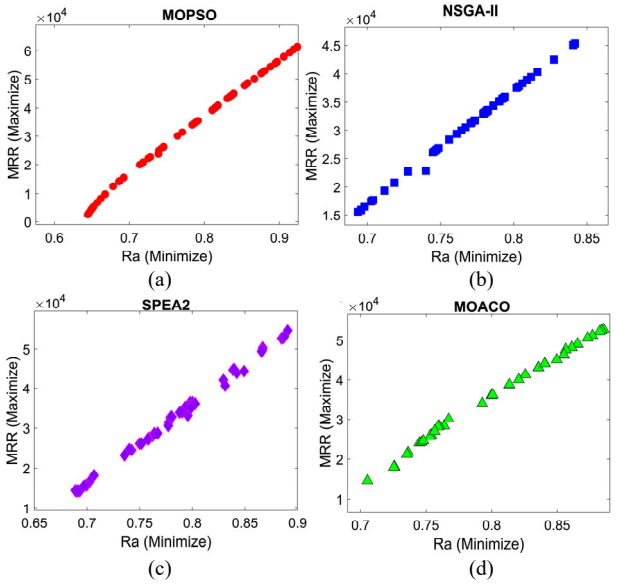

Fig. 7. Pareto optimal front of (a) MOPSO; (b) NSGA-II; (c) SPEA2; and (d) MOACO results.

The convergence results of the algorithms for the two objectives were shown in Fig. 8. The MOPSO algorithm demonstrated the fastest and most stable convergence in minimizing *Ra*, reaching its lowest value early and

maintaining stability throughout the optimization process. NSGA-II showed gradual improvement but with notable fluctuations. However, SPEA2 and MOACO exhibited slower convergence and greater variation in their search for the minimum *Ra*. For MRR, MOPSO also maintained superior performance, consistently achieving its highest MRR value. NSGA-II showed initial improvement but declined before recovering, reaching a lower maximum than MOPSO. SPEA2 and MOACO also show significant oscillations and did not achieve as high or stable an MRR as MOPSO.

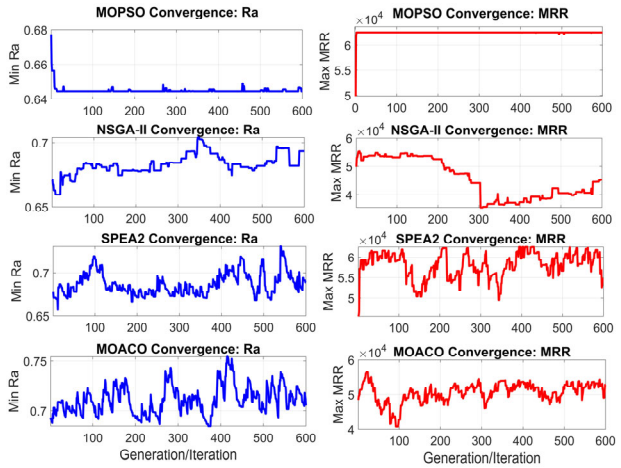

Fig. 8. Convergence results of MOPSO, NSGA-II, SPEA2, and MOACO algorithms.

The rapid convergence of MOPSO may be due to the effective optimization capabilities of the particle swarm optimization method, combined with multi-objective strategies, which allowed it to find extrema and maintain stability quickly. By contrast, NSGA-II showed gradual improvement but experienced fluctuations, possibly because of the Pareto dominance-based selection and supporting diversity in the population. This may be because the algorithm attempted to strike a balance between the two objectives, such that changes in the optimization process became unstable. SPEA2 and MOACO converged more slowly and experienced greater variability, possibly because both algorithms prioritized maintaining diversity in the solution space rather than focusing on fast optimization. The evaluation of solutions based on metrics such as Pareto strength and solution spread caused the convergence process to take longer and remain unstable.

Although MOPSO exhibited fast convergence speed, the optimal values were highly dispersed and unstable for both objectives (Fig. 9). Meanwhile, NSGA-II showed greater concentration in both *Ra* and MRR distributions. Therefore, to prioritize the trade-off between minimizing *Ra* and maximizing MRR, NSGA-II was identified as the most promising algorithm among the four. The concentration of optimal values found by NSGA-II indicated that it produced solutions where *Ra* and MRR were acceptable and stable. Although MOPSO algorithm achieved the highest objective values, it required more careful selection to find balanced solutions within its scattered result set. SPEA2 and MOACO were less effective than NSGA-II in providing well-balanced optimal solutions based on the observed distribution.

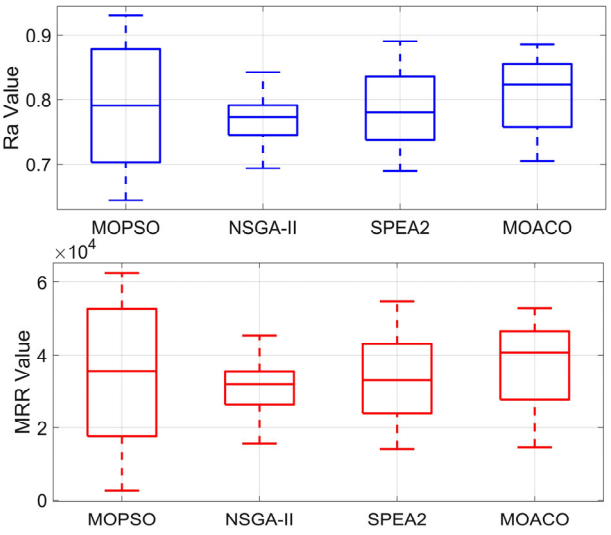

Fig. 9. Distribution of Optimal *Ra* and MRR.

TABLE IV. VALIDATION RESULTS OF MOPSO, NSGA-II, SPEA2 AND MOACO

Algorithm	*S*	*f*	*d*	*Ra*			MRR		
				Opti.	Act.	Dev (%)	Opti.	Act.	Dev (%)
MOPSO	5000.0	0.20	0.50	0.651	0.693	6.06	5,026.6	5,000.0	0.53
	5000.0	0.20	0.25	0.644	0.661	2.50	2,500.0	2,500.0	0.00
	5000.0	1.00	1.25	0.930	1.036	10.24	62,500.0	62,500.0	0.00
NSGA-II	4994.8	0.51	1.24	0.773	0.739	4.60	31,793.4	31,587.1	0.65
	4995.0	0.56	1.25	0.790	0.815	3.07	35,104.5	34,965.0	0.40
	4996.0	0.51	1.25	0.774	0.831	6.86	31,870.2	31,849.5	0.07
SPEA2	4910.8	0.74	1.23	0.849	0.948	10.43	44,393.2	44,393.2	0.00
	4998.0	0.25	1.16	0.689	0.711	3.11	14,352.0	14,352.0	0.00
	4968.8	0.27	1.17	0.697	0.672	3.73	15,490.1	15,490.1	0.00
MOACO	4923.5	0.39	1.13	0.736	0.705	4.43	21,711.1	21,711.1	0.00
	4979.8	0.71	1.22	0.836	0.916	8.78	43,127.3	43,127.3	0.00
	4986.5	0.58	1.18	0.793	0.838	5.39	34,056.2	34,056.2	0.00

Note: The "Act." values of MRR were recalculated using Eq. (1) based on the cutting parameters applied in the confirmation experiments.

D. Validation of Optimization

To evaluate the deviation between the experimentally measured surface roughness and the optimization results of the four algorithms, each Pareto front consisting of 60 optimal solutions was first obtained. From each Pareto front, three solutions were randomly selected for machining experiments to validate *Ra*, while the corresponding *MRR* values were analytically recalculated based on the applied cutting parameters. The random selection was adopted to avoid selection bias and to assess the general reliability of the proposed optimization framework. Based on the validation results summarized in Table IV, a total of twelve validation cases (three per algorithm) were analyzed. The NSGA-II algorithm exhibited a mean deviation of 4.84% for *Ra* and 0.37% for MRR across the validated solutions. Similarly, the MOPSO algorithm showed mean deviations of 6.27% for *Ra* and 0.18% for MRR. The SPEA2 and MOACO algorithms yielded mean deviations of 5.76% and 6.20% for *Ra*, respectively, while maintaining consistently low deviations in the analytically calculated MRR (<0.01%). Although the validation points were randomly selected, the validated solutions collectively spanned different regions of the *Ra* and MRR trade-off space. From a machining physics perspective, these results reflected the inherent compromise between surface quality and productivity governed by feed rate and depth of cut, which influence chip thickness, cutting forces, and surface generation mechanisms. Overall, all algorithms demonstrated low deviations in *Ra* based on experimental validation and consistent values of the calculated MRR, indicating their effectiveness in multi-objective optimization in machining.

IV. Conclusion

This study examined the multi-objective optimization of *Ra* and MRR in the milling of 7075 aluminum alloy using four optimization algorithms. By integrating statistical analysis, predictive modeling, and experimental validation under identical machining conditions, the work provided a comprehensive assessment of algorithmic behavior in a realistic manufacturing context.

The statistical results showed that *S* and *f* significantly influence *Ra*, contributing 20.06% and 79.68%, respectively. In contrast, MRR was primarily governed by *f* and *d*, with contribution ratios of 45.01% and 40.11%, respectively. The GMDH-based predictive model demonstrated high accuracy across eight functional forms, with the two-variable polynomial configuration yielding R^2 values of 0.9990 for training and 0.9962 for validation. In the comparative optimization analysis, NSGA-II produced the most stable and well-distributed Pareto solutions, indicating superior robustness in handling conflicting objectives. Although MOPSO achieved rapid convergence, its solutions were comparatively dispersed, while SPEA2 and MOACO exhibited lower stability in generating balanced trade-off fronts. In addition, the experimental validation results indicated high agreement between the predicted and experimental values, with average deviations of 6.5% for *Ra* and 0.37% for MRR.

Unlike previous studies that often focused on a single optimization technique or lacked integrated experimental verification, this research provides a systematic cross-algorithm comparison combined with statistical contribution analysis and data-driven predictive modeling under consistent machining conditions. Such integration establishes a comprehensive and experimentally validated framework for multi-objective milling optimization, offering both methodological insight and practical guidance for parameter selection in advanced manufacturing. Future studies should investigate more machining parameters as well as other objective functions, to make the optimization framework more adaptable to specific manufacturing conditions.

Conflict of Interest

The authors declare no conflict of interest.

Author Contributions

VTP and CCT contributed to the study conception and design. VTT and SH performed the analysis and interpretation of the results. CCT and VTT wrote the manuscript; all authors reviewed and approved the final manuscript.

Acknowledgement

The authors sincerely appreciate the invaluable support provided by the Faculty of Electronics Engineering 1 at the Posts and Telecommunications Institute of Technology (PTIT), Hanoi, Vietnam, in the completion of this study. The authors would also like to express their sincere gratitude to the anonymous reviewers and editors for their invaluable comments and suggestions, which have greatly contributed to the improvement of this work.

References

[1] L. G. De Oliveira, A. P. de Paiva, P. P. Balestrassi *et al.,* "Response surface methodology for advanced manufacturing technology optimization: Theoretical fundamentals, practical guidelines, and survey literature review," *International Journal of Advanced Manufacturing Technology*, vol. 104, no. 5, pp. 1785–1837, 2019.

[2] M. H. El-Axir, M. M. Elkhabeery, and M. M. Okasha, "Modeling and parameter optimization for surface roughness and residual stress in dry turning process," *Engineering, Technology & Applied Science Research*, vol. 7, no. 5, pp. 2047–2055, 2017.

[3] Y. Zheng, Y. Tian, J. Ma *et al.,* "Residual stress formation mechanism considering cutting energy in milling of 7075 aluminum alloy," *International Journal of Advanced Manufacturing Technology*, vol. 131, no. 5, pp. 3039–3055, 2024.

[4] M. Tajally and E. Emadoddin, "Mechanical and anisotropic behaviors of 7075 aluminum alloy sheets," *Materials & Design*, vol. 32, no. 3, pp. 1594–1599, 2011.

[5] C. C. Tran, V. T. Luu, V. T. Nguyen *et al.,* "Multi-objective optimization of CNC milling parameters of 7075 aluminium alloy using response surface methodology," *Jordan Journal of Mechanical and Industrial Engineering*, vol. 17, no. 3, 2023.

[6] I. Rahimi, A. H. Gandomi, F. Chen *et al.,* "A review on constraint handling techniques for population-based algorithms: From single-objective to multi-objective optimization," *Archives of Computational Methods in Engineering*, vol. 30, no. 3, pp. 2181–2209, 2023.

[7] K. Diao, X. Sun, G. Bramerdorfer *et al.,* "Design optimization of switched reluctance machines for performance and reliability enhancements: A review," *Renewable and Sustainable Energy Reviews*, vol. 168, no. 112785, 2022.
[8] R. Kumar, S. Singh, P. S. Bilga *et al.,* "Revealing the benefits of entropy weights method for multi-objective optimization in machining operations: A critical review," *Journal of Materials Research and Technology*, vol. 10, pp. 1471–1492, 2021.
[9] J. F. Arinez, Q. Chang, R. X. Gao *et al.,* "Artificial intelligence in advanced manufacturing: Current status and future outlook," *Journal of Manufacturing Science and Engineering*, vol. 142, no. 11, 110804, 2020.
[10] R. Vyasa, P. Brahmbhatt, C. Sonawane *et al.,* "Investigation on the multi-objective optimization of machining parameters and prediction for EN series materials," *Engineering, Technology & Applied Science Research*, vol. 14, no. 5, pp. 16427–16437, 2024.
[11] D. E. Ighravwe and S. A. Oke, "Machining performance analysis in end milling: Predicting using ANN and a comparative optimisation study of ANN/BB-BC and ANN/PSO," *Engineering Journal*, vol. 19, no. 5, pp. 121–137, 2015.
[12] Y. Zhang, Y. Liu, X. Zhang *et al.,* "Multi-objective particle swarm optimization with integrated fireworks algorithm and size double archiving," *Int. J. Comput. Intell. Syst*., vol. 18, no. 2, pp. 1–37, 2025.
[13] S. Lalwani, S. Singhal, R. Kumar *et al.,* "A comprehensive survey: Applications of Multi-Objective Particle Swarm Optimization (MOPSO) algorithm," *Transactions on Combinatorics*, vol. 2, no. 1, pp. 39–101, 2013.
[14] V. T. Tran, T. L. Nguyen, C. C. Tran *et al.,* "Multi-objective optimization of surface roughness and material removal rate in turning SKD11 steel: A combination of GP and MOPSO algorithms," *Engineering Journal*, vol. 29, no. 8, pp. 135–145, 2025.
[15] S. Verma, M. Pant, and V. Snasel, "A comprehensive review on NSGA-II for multi-objective combinatorial optimization problems," *IEEE Access*, vol. 9, pp. 57757–57791, 2021.
[16] C. C. Tran, "Optimization of filling time and volumetric shrinkage rate in simulation of plastic product injection molding process using RSM and NSGA-II," *Jordan Journal of Mechanical and Industrial Engineering*, vol. 19, no. 1, pp. 67–77, 2025.
[17] R. K. Ghadai, A. Baraily, K. Logesh *et al.,* "Objective optimization of drilling of hybrid aluminium metal matrix composites using ANN NSGA-II hybrid approach," *International Journal on Interactive Design and Manufacturing*, vol. 19, no. 7, pp. 1–12, 2024.
[18] X. Liu and D. Zhang, "An improved SPEA2 algorithm with local search for multi-objective investment decision-making," *Applied Sciences*, vol. 9, no. 8, 1675, 2019.
[19] E. Chołodowicz and P. Orłowski, "Comparison of SPEA2 and NSGA-II applied to automatic inventory control system using hypervolume indicator," *Studies in Informatics and Control*, vol. 26, no. 1, pp. 67–74, 2017.
[20] M. A. Awadallah, S. N. Makhadmeh, M. A. Al-Betar *et al.,* "Multi-objective ant colony optimization: Review," *Archives of Computational Methods in Engineering*, vol. 32, no. 2, pp. 995–1037, 2025.
[21] C. Guo, X. Chen, Q. Li *et al.,* "Milling optimization of GH4169 nickel–based superalloy under minimal quantity lubrication condition based on multi-objective particle swarm optimization algorithm," *The International Journal of Advanced Manufacturing Technology*, vol. 123, no. 11, pp. 3983–3994, 2022.
[22] C. J. Luis-Pérez, "Multi-objective optimization of electrical discharge machining parameters using particle swarm optimization," *Applied Soft Computing*, vol. 153, 111300, 2024.
[23] C. C. Tran, "Modelling and optimization of surface roughness and material removal rate in milling SKD11 using GMDH and NSGA-II," *International Journal of Mechanical Engineering and Robotics Research*, vol. 13, no. 6, pp. 618–627, 2024.
[24] X. Lu, Y. Zhang, Z. Sun *et al.,* "Multi-objective optimization of cutting parameters for micro-milling nickel-based superalloy thin-walled parts based on improved NSGA-II algorithm," *International Journal of Advanced Manufacturing Technology*, vol. 135, no. 1, pp. 775–786, 2024.
[25] Y. Yang, Y. Liu, Y. Wang *et al.,* "Optimization of complex surface milling parameters based on HSS-MFM and OBL-NSGA-II," *International Journal of Intelligent Robotics and Applications*, vol. 9, no. 2, pp. 1–28, 2024.
[26] H. Ma, Y. Zhang, S. Sun *et al.,* "A comprehensive survey on NSGA-II for multi-objective optimization and applications," *Artificial Intelligence Review*, vol. 56, no. 12, pp. 15217–15270, 2023.
[27] A.-T. Nguyen, V.-H. Nguyen, T.-T. Le *et al.,* "A hybridization of machine learning and NSGA-II for multi-objective optimization of surface roughness and cutting force in AISI 4340 alloy steel turning," *Journal of Machine Engineering*, vol. 23, no. 1, pp. 133–153, 2023.
[28] F. Ziyad, H. Alemayehu, D. Wogaso *et al.,* "Multi-objective optimization of machining parameters of mild steel AISI 1018 under compressed air-assisted cooling by using genetic algorithm," *International Journal on Interactive Design and Manufacturing*, vol. 19, pp. 5291–5311, 2024.
[29] C. C. Tran, T. T. Nguyen, and V. T. Nguyen, "Multi-objective optimisation in turning AISI 304 stainless steel: An integration of the Taguchi method, response surface methodology, and NSGA-II," *International Journal of Industrial and Systems Engineering*, vol. 50, no. 3, pp. 413–432, 2025.
[30] K. Amouzgar, S. Bandaru, T. Andersson *et al.,* "A framework for simulation-based multi-objective optimization and knowledge discovery of machining process," *The International Journal of Advanced Manufacturing Technology*, vol. 98, no. 9, pp. 2469–2486, 2018.
[31] H. Wang, Y. Du, and F. Chen, "A hybrid strategy improved SPEA2 algorithm for multi-objective web service composition," *Applied Sciences*, vol. 14, no. 10, 4157, 2024.
[32] A. Naik. "Multi-objective social group optimization for machining process," *Evolutionary Intelligence*, vol. 17, no. 3, pp. 1655–1676, 2024.
[33] N. Rana, M. S. Abd Latiff, S. M. Abdulhamid *et al.,* "A hybrid whale optimization algorithm with differential evolution optimization for multi-objective virtual machine scheduling in cloud computing," *Engineering Optimization*, vol. 54, no. 12, pp. 1999–2016, 2022.
[34] A. G. Ivakhnenko, "Polynomial theory of complex systems," *IEEE Transactions on Systems, Man, and Cybernetics*, no. 4, pp. 364–378, 1971.
[35] Y. Yusoff, M. S. Ngadiman, and A. M. Zain, "Overview of NSGA-II for optimizing machining process parameters," *Procedia Engineering*, vol. 15, no. pp. 3978–3983, 2011.
[36] N. Shahabi Sani, M. Manthouri, and F. Farivar. "A multi-objective ant colony optimization algorithm for community detection in complex networks," *Journal of Ambient Intelligence and Humanized Computing*, vol. 11, no. 1, pp. 5–21, 2020.
[37] C. A. C. Coell and M. S. Lechuga, "MOPSO: A proposal for multiple objective particle swarm optimization," in *Proc. the 2002 Congress on Evolutionary Computation*, 2002, vol. 2, pp. 1051–1056.
[38] K. Deb, A. Pratap, S. Agarwal *et al.,* "A fast and elitist multiobjective genetic algorithm: NSGA-II," *IEEE Transactions on Evolutionary Computation*, vol. 6, no. 2, pp. 182–197, 2002.
[39] E. Zitzler, M. Laumanns, and L. Thiele, "SPEA2: Improving the strength Pareto evolutionary algorithm," *TIK Report*, vol. 103, 2001.
[40] D. Angus and C. Woodward, "Multiple objective ant colony optimisation," *Swarm Intelligence*, vol. 3, no. 1, pp. 69–85, 2009.